



Contents lists available at ScienceDirect

Nuclear Inst. and Methods in Physics Research, A

journal homepage: www.elsevier.com/locate/nima

Four-harmonic buncher for radioactive and stable beams switching at the ATLAS facility

S.V. Kutsaev^{a,*}, A.Yu. Smirnov^a, R. Agustsson^a, D. Chao^a, S. Lynam^a, B. Mustapha^b, S. Sharamentov^b^a RadiaBeam Technologies LLC, 1717 Stewart St, Santa Monica, CA 90403, USA^b Argonne National Laboratory, 9700 S. Cass Ave, Lemont, IL 60439, USA

ARTICLE INFO

Keywords:

Linear accelerator
Buncher
RFQ
Coaxial resonator
Multi-harmonic signal
Heavy ions
ATLAS

ABSTRACT

The Argonne Tandem Linac Accelerator System (ATLAS) is planning an upgrade to a multi-user facility to simultaneously accelerate both stable beams from an ECR ion source and radioactive beams from an Electron Beam Ion Source charge breeder. The ATLAS Multi-User Upgrade will need to provide high transmission of ion beams with a mass-to-charge ratio up to 7 as it enables more options to alternate radioactive and stable beams. Currently, the bunching is provided with a lumped circuit multi-harmonic buncher, which cannot effectively operate at the required amplitude of the saw-tooth voltage for ions with mass-to-charge ratio of 7 due to thermal issues.

RadiaBeam Systems in collaboration with Argonne National Laboratory has designed a four-harmonic coaxial resonator buncher with the ATLAS fundamental frequency of 12.125 MHz, and a compact, less than 2-m-long, footprint, capable of providing the required voltage of 6.2 kV. This device allows fast and reliable pre-bunching of DC ion beams with the capability of fast switching of heavy-ion radioactive and stable beams for delivery to multiple users. In this paper, we will discuss the RF and engineering design considerations of this buncher.

1. Introduction

The Argonne Tandem Linac Accelerator System (ATLAS) [1] is the US DOE National User Facility for stable low-energy heavy ion beams. With the recent commissioning of the Californium Rare Isotope Breeder Upgrade (CARIBU) [2,3], ATLAS is also being used to accelerate radioactive ions. There are plans [4] to convert ATLAS into a multi-user facility to simultaneously accelerate both stable beams from the ECR ion source [5] and radioactive beams from an Electron Beam Ion Source (EBIS) [6]. The EBIS, which has been operating for about two years, is a charge breeder for CARIBU. Radioactive beams produced from EBIS have A/q between 4 and 7 (where A is the atomic mass number and q is the charge state) and can be injected into ATLAS in short pulses.

One of the key goals of the ATLAS Multi-User Upgrade [7] is to provide high transmission of ion beams with A/q up to 7 for efficient use of the multi-user facility at ATLAS, as it provides more options to alternate radioactive and stable beams. Currently, the bunching is provided by a lumped circuit multi-harmonic buncher (MHB), which cannot effectively operate at the required voltage amplitude of 6.2 kV for ions with $A/q=7$ due to thermal issues [8].

The ATLAS Positive Ion Injector [9] was developed in the early 1990's to provide beams of heavy ions up to, and including, ^{238}U for the ATLAS research program in low-energy nuclear physics. Later, a continuous wave radio-frequency quadrupole (CW RFQ) capable of accelerating any ion from proton to uranium from 30 keV/u to 295 keV/u was designed and built [10]. For such a linac system, to produce a small longitudinal beam emittance and avoid beam loss in the superconducting linac, the ion beams must be pre-bunched for injection into the first RF accelerator with an MHB. The MHB system for ATLAS was developed long ago [11] and has been successfully operated for decades. The original MHB was upgraded more than ten years ago to a four-harmonic lumped-element resonant structure loaded with parallel grids [12]. The use of two grids reduced the beam transmission by about 20%, which is unacceptable in the acceleration of secondary radioactive beams. With the progress in the development of radioactive ion beams at ATLAS, the MHB grids were replaced with a grid-less bunching system [13].

For heavy ions, the “effective” voltage scales as A/q . When the A/q ratio is large, the buncher voltage (V) should be increased accordingly to maintain the bunching efficiency. The dissipation power (P)

* Corresponding author.

E-mail address: kutsaev@radiabeam.com (S.V. Kutsaev).<https://doi.org/10.1016/j.nima.2018.07.054>

Received 19 June 2018; Received in revised form 18 July 2018; Accepted 18 July 2018

Available online xxxx

0168-9002/© 2018 Elsevier B.V. All rights reserved.

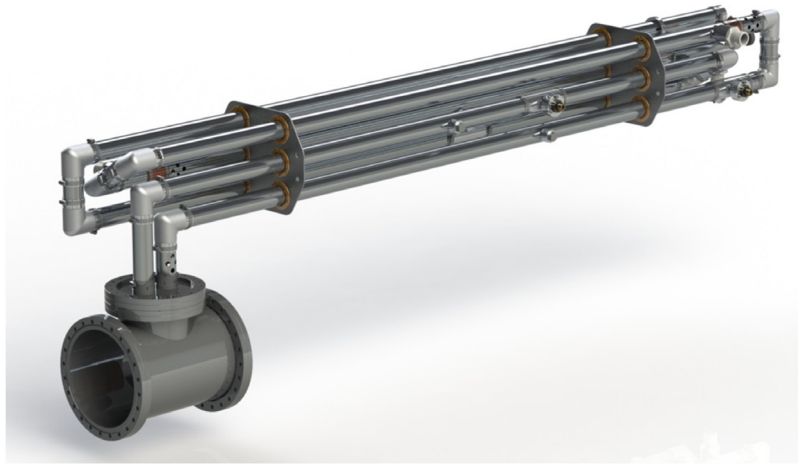


Fig. 1. Conceptual design of the 12.125 MHz four-harmonic MHB.

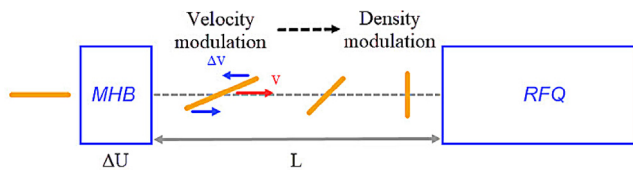


Fig. 2. Schematics of MHB operation principle. Here, the bunch is represented by the solid line, v is the beam velocity, Δv is the velocity change of the end particles due to the applied voltage ΔU , L is the distance between MHB and RFQ.

scales as $P \sim V^2$, so thermal issues become significant for a multi-kV lumped-circuit MHB. The existing buncher based on lumped elements cannot provide the 6.2 kV voltage required for the efficient bunching of ion beams with an A/q of 7, since it is unable to handle powers higher than 180 W, due to the temperature shift of resonant frequencies. Thus, the development of a new resonator-based buncher to replace the lumped-circuit structure is the best solution to this limitation.

Some resonator-based MHBs have already been developed, with the most recent example at FRIB [14]. However, this buncher is based on Quarter-Wave-Resonator (QWR) cavities and can only produce three harmonics. The harmonics existing in QWRs are odd (1, 3, 5 etc.), so it is easy to get 1st and 3rd harmonics. The second QWR is designed for the frequency twice as high as the first harmonic, i.e. it provides the harmonics numbers multiplied by factor of 2, relative to the first QWR (2, 6, 10 etc.). Therefore, the 4th harmonic is missing in such two-QWRs system. Another problem is the overall cavity dimensions. The operating frequencies of the existing QWR-based MHBs are several times higher compared to what is required for ATLAS. For example, the FRIB MHB operates at 40 MHz (1st harmonic). Since the fundamental frequency of ATLAS is 12.125 MHz, the length of a $\lambda/4$ coaxial resonator would be 6 m if the FRIB design is directly scaled, which is unacceptably large for construction and integration into the ATLAS beamline.

Also, the new buncher is required for the effective switching of radioactive and stable beams and must operate in “dual-” or “interlaced-” energies regime, when each even beam pulse (radioactive) is accelerated to one energy and each odd pulse (stable beam) to another energy. Therefore, peak-to-peak voltage is switched for the duration of the radioactive beam pulse.

In response to these requirements, RadiaBeam Systems in collaboration with Argonne National Laboratory has designed a four-harmonic coaxial resonator buncher, shown in Fig. 1, with a fundamental frequency of 12.125 MHz and with compact, less than 2 m, footprint capable of providing the required voltage. This device allows fast and

Table 1

Design parameters of the 12.125 MHz multi-harmonic buncher.

| Parameter | Value |
|-------------------------------|-------------|
| Frequency of the 1st harmonic | 12.125 MHz |
| Number of harmonics | 4 |
| Effective voltage | 6200 V |
| Total RF power | 175 W |
| Beam energy | 30.5 keV/u |
| Maximum A/q | 7 |
| Distance to RFQ | 5.48 m |
| Coaxial size | 1-5/8" |
| Coaxial impedance | 87 Ω |

reliable pre-bunching of DC ion beams with the capability of fast switching of heavy-ion radioactive and stable beams for delivery to multiple users.

In this paper, we will present the physical and conceptual engineering design of the buncher. The parameters of the developed MHB are summarized in Table 1. The optimized design offers several attractive features:

- The use of standard coaxial lines allowing a significant reduction in fabrication costs;
- Higher impedance and smaller dimension of coaxial line reduced the required power and made the design more compact;
- Optimized the electrode shape and the distribution of harmonic power losses, due to the transit time factor, allowed to increase the beam aperture by a factor of two with only 20% increase in power;
- Optimization of power losses allowing integration with the existing ATLAS power and LLRF systems with minimal upgrade;
- The designed tuning mechanisms permit precise and remote tuning of the cavity;
- The cooling system allows thermal and frequency stability of the cavity;
- The cavity can rapidly, within 50 μ s, switch the voltage for different beam species to allow the effective switching of radioactive and stable beams.

2. RF design of the buncher

The voltage required for bunching is found by solving the problem described in Fig. 2. Assume that the particles travel with an average energy W_0 and the corresponding velocity $v = \beta c$. At the time $t = 0$, they arrive at the buncher gap that provides a linear energy-phase correlation

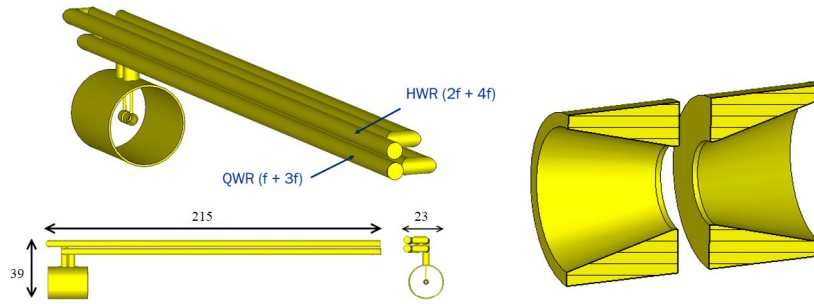


Fig. 3. MHB resonators (left) and electrodes (right). QWR ($f + 3f$) and HWR ($2f + 4f$) correspond to the quarter-wave and half-wave resonators respectively, see details in text. All dimensions are in centimeters.

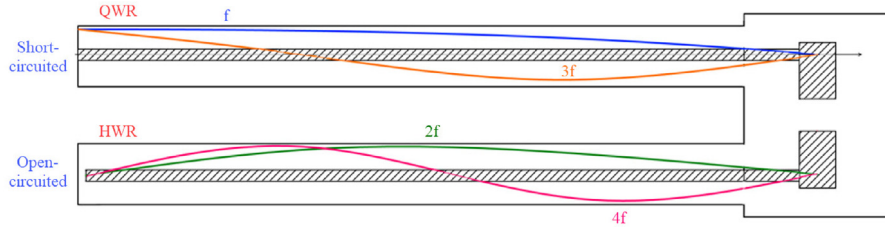


Fig. 4. MHB schematics and magnetic field profiles along resonators axes.

Table 2

Extracted harmonics and boundary conditions of each resonator.

| Frequency, MHz | Resonator number | Number of wavelengths | Boundary condition |
|----------------|------------------|-----------------------|--------------------|
| 12.125 | 1 | $1/4$ | Short-circuited |
| 24.250 | 2 | $1/2$ | Open-circuited |
| 36.375 | 1 | $3/4$ | Short-circuited |
| 48.500 | 2 | 1 | Open-circuited |

with a maximal amplitude ΔU at the frequency F_0 ($\lambda = c/F_0$). After traveling the distance L , the beam is phase-focused into the RFQ.

The voltage signal composed of four harmonics is given by [11]:

$$U_0(t) = U_1 \cdot [\sin(\omega t) - 0.4 \cdot \sin(2\omega t) + 0.18 \cdot \sin(3\omega t) - 0.06 \cdot \sin(4\omega t)] \quad (1)$$

For the ATLAS parameters: $W_0 = 30$ keV/u, $L = 5$ m, and $f_0 = 12.125$ MHz, we found that to effectively bunch the particles with A/q up to 7, the buncher must provide a 1st harmonic voltage of $U_1 = 5000$ V and a total voltage of $U_0 = 6200$ V. The actual amplitudes should be adjusted for the particular ion beam species during the beam dynamics simulation.

Once the required voltage was defined, we developed the RF design of the MHB made of two coaxial resonators folded in three sections and two accelerating electrodes placed inside a cylindrical vacuum chamber as shown in Fig. 3. The shapes of the electrodes are identical to those used in the current ATLAS MHB. The goal of the RF design is to create a device combining the first four harmonics of the fundamental frequency 12.125 MHz to form a saw-tooth voltage pulse across the accelerating gap.

The accelerating electrodes represent an open boundary for the coaxial resonators. Thus the second boundary condition at each coaxial resonator end should match the EM-fields profiles of the corresponding resonances, as shown in Table 2.

The harmonic combination principle is based on two coaxial resonators (one is used for odd harmonics f and $3f$, and the other for even harmonics $2f$ and $4f$) as shown in Fig. 4. We name these resonators in accordance with the resonance type of the lowest frequency – quarter-wave (QWR) and half-wave (HWR) resonators.

As the axial lengths of both resonators are approximately 6 m (quarter-wavelength of the fundamental harmonic, and half-wave of

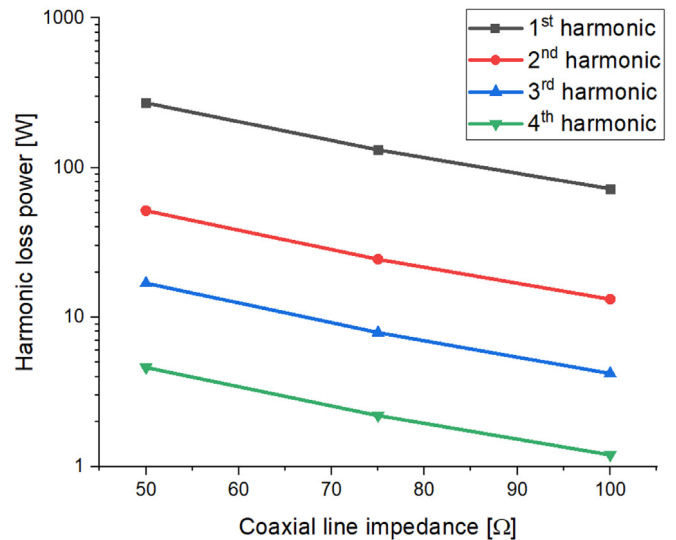


Fig. 5. Power requirements for each harmonic as a function of resonators impedances, as simulated in CST MWS.

the second harmonic, respectively), they must be folded, as shown in Fig. 3 to ensure overall system compactness. The coaxial transverse dimensions are chosen according to the Electronic Components Industry Association (ECIA) EIA standards [15] ($7/8''$, $1-5/8''$ and $3-1/8''$). We have chosen the outer pipe diameter as EAI $1-5/8''$ to minimize the overall dimensions since the designed cavity must fit in the tight space of the ATLAS beamline. The inner conductor was chosen to be $7/8''$, as this combination gives a line impedance of $\sim 87 \Omega$ which leads to lower power requirements than the 50Ω case, as shown in Fig. 5.

We performed electromagnetic simulations in CST Microwave Studio (CST MWS) [16] to estimate the required power. In these simulations, we have only estimated the power losses in the resonators, and the model did not include power couplers. The calculated electric field distribution near the electrodes is shown in Fig. 6. It is clearly seen that the field is not symmetric and there is residual field outside the electrodes, which will influence the total voltage effective energy gain

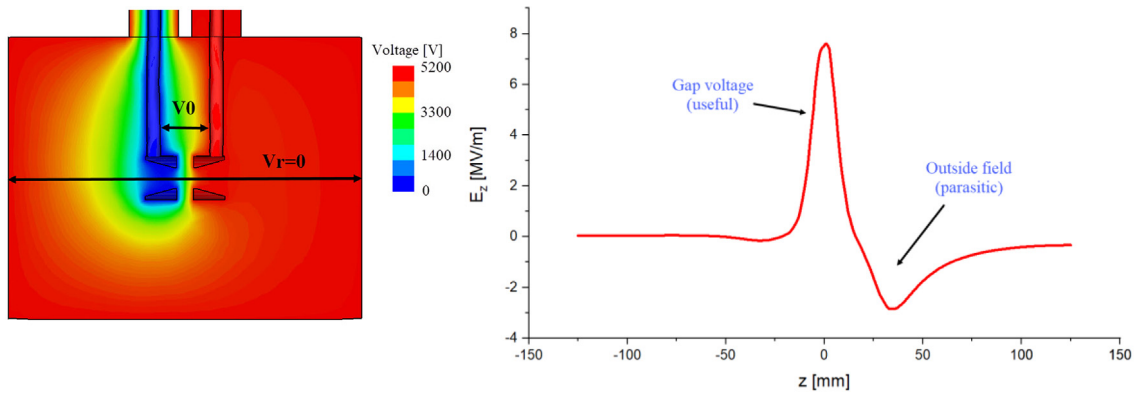


Fig. 6. Electric field 2D (left) and on-axis (right) distributions for the first harmonic.

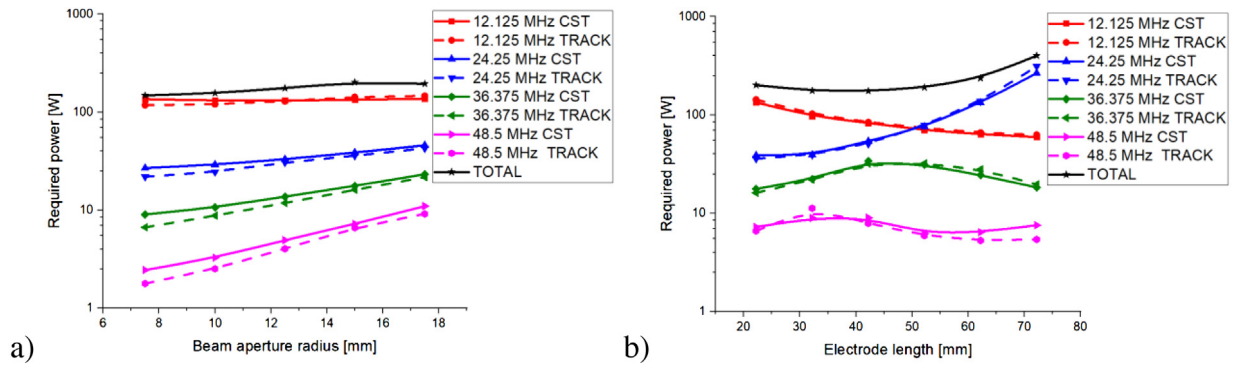


Fig. 7. Required harmonics power as a function of the electrode dimensions (a – aperture, b – length). An aperture radius of 15 mm was used in the simulations presented in (b). Some discrepancies between CST and TRACK come from the fact that CST uses formula (2) to estimate voltage, while TRACK accurately calculates the beam dynamics.

(V):

$$V = \int_{-L/2}^{L/2} E_z(z) e^{ik_z z} dz \quad (2)$$

where L is the vacuum chamber length, z is the coordinate along the chamber axis, E_z is the longitudinal coordinate of the electric field, and k_z is the wave-number. Since the particles travel with a finite velocity, the phase of RF field changes during the time of flight (so called transit time factor). Thus, it is possible to optimize the electrode shape, so that the effect of field asymmetry is minimized as described below.

Along with the EM simulations, we performed beam dynamics simulation using the TRACK code [17] to verify that the calculated voltage is indeed correct and provides the maximum compression of the beam. Fig. 7 demonstrates the process of electrodes' shape optimization. First, we increased the beam aperture radius by 50%: from 10 to 15 mm to allow acceleration of higher intensity beams. Next, we optimized the length of the electrode, so that the power requirements are minimized. Since the transit-time-factor effect is different for each harmonic, we were able to reduce its influence for the first, strongest harmonic, at the cost of the higher power requirements of higher harmonics, which are much weaker. The optimization results are summarized in Table 3. Even by increasing the beam aperture by 50%, we were able to keep the required power level within 6% above the original value.

Since the designed MHB will be used for the switching of beams, we performed TRACK beam dynamics analysis in the ATLAS front-end (Fig. 8) for three species of particles with different A/q ratios and beam currents ($^{238}\text{U}^{34+}$, $^{40}\text{Ar}^{10+}$ and protons) as shown in Table 4. The comparison of simulation results with the original and the optimized MHB are provided in Figs. 9 and 10 and demonstrate that the designed MHB is capable of providing good beam quality for both high A/q particles (practically impossible in current ATLAS MHB due to the heating limitations), and for high-current beams.

Table 3

Comparison of the original and optimized electrodes design.

| Parameter | Original electrodes | New electrodes |
|------------------------|---------------------|----------------|
| Beam hole diameter, mm | 10 | 15 |
| Electrode length, mm | 22.2 | 42 |
| Power (F0), W | 121 | 84 |
| Power (2F0), W | 29 | 51 |
| Power (3F0), W | 12 | 32 |
| Power (4F0), W | 4 | 8 |
| Total power, W | 166 | 175 |

Table 4

Beam parameters of different simulated ion beams.

| Ions | $^{238}\text{U}^{34+}$ | $^{40}\text{Ar}^{10+}$ | p^+ |
|----------------------------|------------------------|------------------------|--------------|
| A/q | 7 | 4 | 1 |
| Input energy, keV/u | 30.5 | 30.5 | 30.5 |
| Current, mA | 0 | 0.1 | 0.25 |
| Transmission after RFQ, % | 80.6 | 81.5 | 84.8 |
| $\epsilon_{x,y}$, cm mrad | 0.12 | 0.12 | 0.12 |
| $\alpha_{x,y}$ | 1.0 | 1.0 | 1.0 |
| $\beta_{x,y}$, cm/rad | 100 | 100 | 100 |
| ϵ_z , deg % | 25.0 | 25.0 | 25.0 |
| α_z | 0.0 | 0.0 | 0.0 |
| β_z , deg/% | 10.0 | 10.0 | 10.0 |
| Sawtooth MHB voltage, V | 5675 | 3242 | 942 |

3. Design of the RF components

We have performed the design of the cavity subsystems such as power couplers and tuners required for the MHB operations. We use inductive couplers to drive the resonators. Coupler loop designs have to be optimized to provide the coupling strength for each harmonic slightly above the critical coupling ($\chi = 1.0-1.1$) to avoid power reflections and

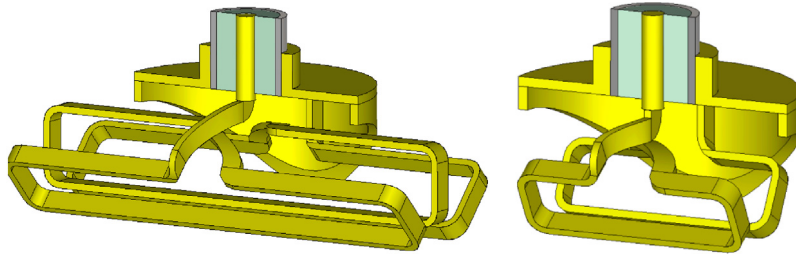


Fig. 11. 3D models of coupling loops for the 1st (left) and 4th harmonics.

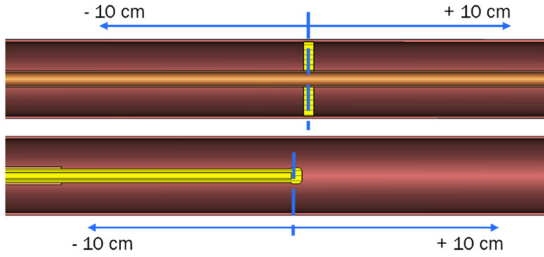


Fig. 12. Coarse tuners: sliding plunger for QWR (top) and telescopic inner conductor extender for HWR (bottom). Moveable parts are highlighted .

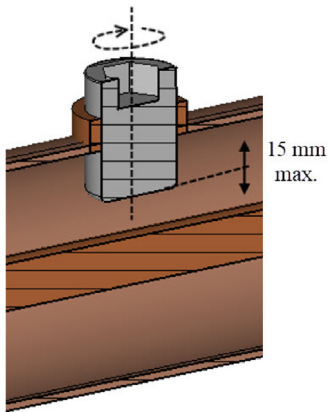


Fig. 13. Design of the tuning screw.

Table 5
Screw tuners positions and sensitivities.

| Tuner harmonic (f_a) # | 1 | 2 | 3 | 4 |
|-----------------------------|-------|------|-------|------|
| Second harmonic (f_b) # | 3 | 4 | 1 | 2 |
| Tuner position, m | 4.584 | 1.21 | 1.366 | 2.38 |
| df_a/dx , kHz/mm | -2.7 | -4.0 | -7.0 | -6.4 |
| Δf_a , kHz | -38 | -55 | -96 | -90 |

operation in the under-coupled regime. The coupler should also allow ± 0.1 coupling adjustment. We used the square loop design from FRIB MHB [18] as a starting point for the design. The analytical expression for the inductive coupling coefficient is [19]:

$$\chi = \frac{(\omega\mu_0 \cos \theta)^2 H^2}{2Z_0 P_L} \quad (3)$$

where $\omega = 2\pi f_0$, $Z_0 = 50 \Omega$ (generator impedance), H is the magnetic field magnitude averaged over loop area A , θ is the angle between the A and H vectors and P_L is the RF power loss in the cavity.

Assuming loops to be placed at magnetic field maximums for each resonant mode and orthogonal to magnetic field ($\cos \theta = 1$) and using H^2/P_L values obtained from CST simulations for current QWR and HWR

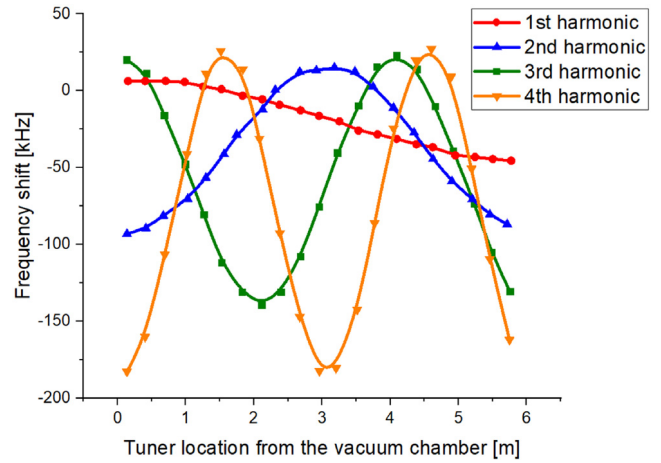


Fig. 14. Frequency sensitivities as a function of screw tuner position along the coaxial resonator ($z = 0$ is the position of the vacuum chamber with electrodes).

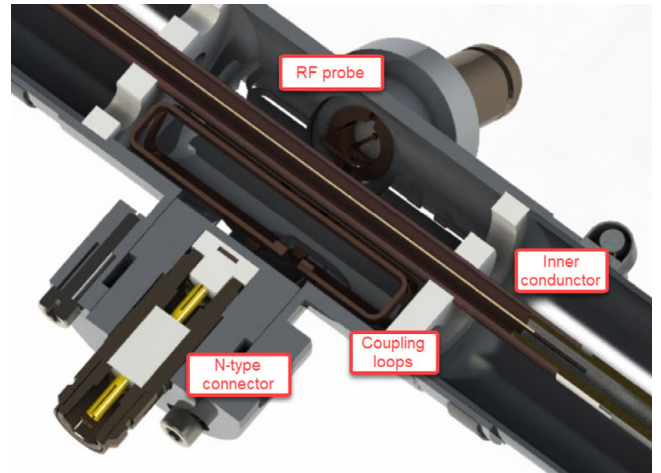


Fig. 15. Coupling loops and RF probe.

geometries, the loop areas for $\chi = 1.1$ were calculated. Due to the limitation of vertical loop size, the loops were folded into triple turns for the 1st and 2nd harmonics, and double turns for the 3rd and 4th harmonics. The optimized coupler shapes are shown in Fig. 11.

The N-type coaxial input to each coupler along with rotational adjustability has sliding ability to change the loop insertion depth for individual coupling adjustments. To prevent cross-talking between the RF sources, each solid-state amplifier must be equipped with a filter that would stop the unwanted harmonics. Such filters have been designed and will be described in the following sections.



Fig. 16. HWR and QWR coarse tuning mechanisms.

We made two types of tuners for frequency adjustment – coarse and fine. Coarse tuners are represented by a sliding plunger in QWR and a telescopic inner conductor extender in HWR, see Fig. 12.

Coarse frequency tuning will cause some coupling coefficient change. Changing the resonators lengths will shift the magnetic field maximums from coupler positions. The loop will ‘see’ changes to the H -value proportional to $\cos(N \cdot \pi \cdot \Delta z/L)$, where N is the harmonic number, Δz is the maximum shift of 10 cm and L is the resonator length of 6 m. Since $\chi \sim H^2$, this results in a change in χ of 0.3% at 12.125 MHz, 1.1% at 24.25 MHz, 2.4% at 36.375 MHz and 4.8% at 48.5 MHz. These coupling distortions can be compensated with coupler depth adjustment.

The second type of tuners will be made of four $\varnothing 15$ mm screws in the outer conductor, shown in Fig. 13. The plots of frequency shift as a function of screw positions along the coaxial resonators, simulated using the maximum penetration depth of 15 mm for the screw tuners, are presented in Fig. 14. We select the tuners positions such as each of them causes zero frequency shift of one mode in the resonator and non-zero of the other, as shown in Fig. 14 and Table 5. Four RF probes for monitoring the amplitude and phase of each harmonic will be placed close to the corresponding RF power coupler. These probes have the shape of a 10×4 mm single-turn loop with the N-type connector.

4. Conceptual engineering design

The primary objective of the conceptual engineering design of the resonators was to fully meet all design objectives while keeping costs low by utilizing as many off-the-shelf components as possible. By using the EIA 1-5/8" standard transmission line for the outer conductor portion and the EIA 7/8" standard for the inner conductor, the only custom components required for the primary parts of the resonator structure are the insulating spacers used to suspend the inner conductor within the outer conductor. Other custom components required for the resonator are the coupling antennas, the tuning mechanisms, the forced air inlets and outlets, the mounting plates and the RF electrodes, which are discussed below.

Overall, the structure is very simple, comprised of three legs and two “switchback” sections for each resonator to keep the overall footprint of the device low. These sections are then folded into themselves and assembled within mounting plates, which maintain the spacing and alignment of each resonator. The legs are directly inserted into bronze bushings to permit low friction growth axially. These plates can be easily mounted either to a stand from below or suspended from above, depending on space requirements and mechanical attachments.

Several custom components and modifications were added to the outer conductor portion of the resonators to fully realize the design’s

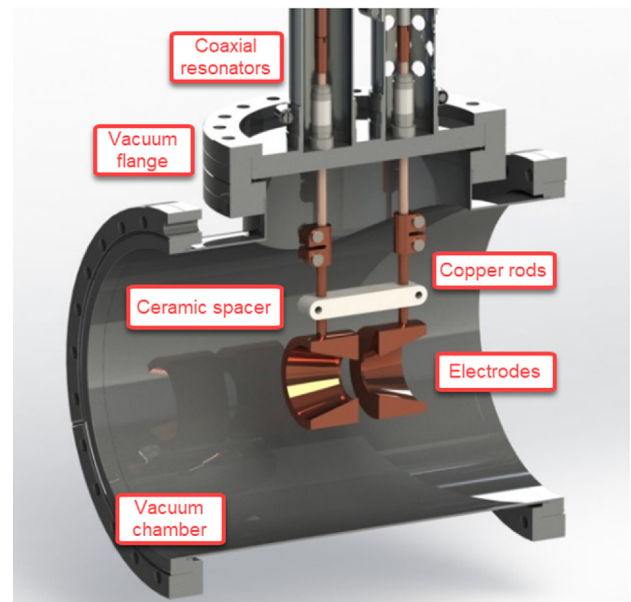


Fig. 17. Beamline chamber and electrodes.

functionality. Installation of the coupling loops was achieved by creating an independent section of the conductor which houses both the coupling loops as well as the RF probes, which are adjustable radially towards the center conductor and azimuthally around the axis of the feedthroughs to optimize the coupling. This is then locked into place with a brass-tipped set screw located on the side of their respective housing. Both utilize type-N jacks, which provide a universal connection. The engineering design of coupling loops and RF probe is shown in Fig. 15.

There are two primary methods of coarse mechanical tuning in the structures as shown in Fig. 16. The first involves directly adjusting the length of the resonating cavity using a copper shorting disc. In the quarter wave resonator, garter springs mounted to this disc provide the electrical path between inner and outer conductors. Adjustment is achieved by a simple tuning knob which slides the position of the shorting disk by up to 25 mm full travel. In the HWR, a collar can be mechanically coupled to the telescopic inner conductor extender through the end cap of the line to adjust its extension over 25 mm full travel. Both adjustments are secured by a brass-tipped set screw.

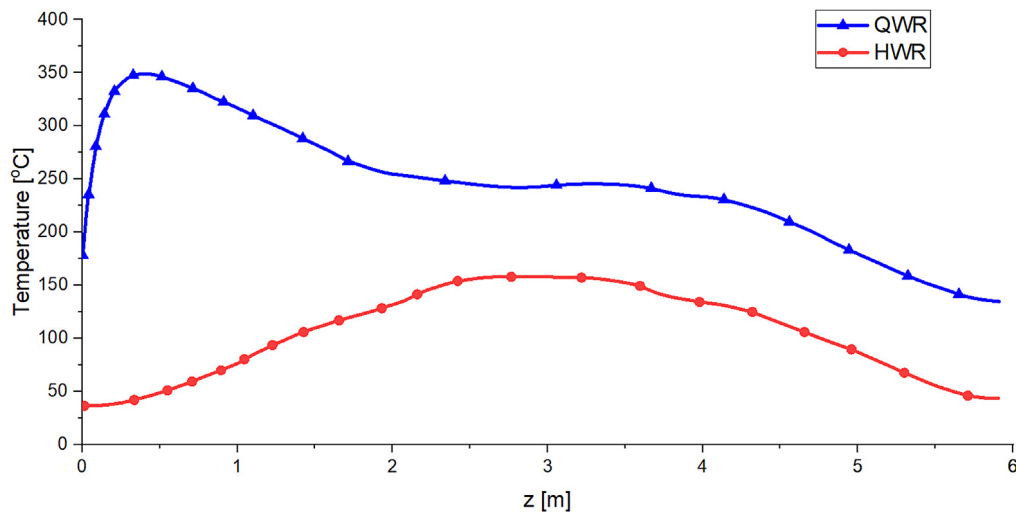


Fig. 18. Temperature distribution on the central conductors of QWR and HWR with a 175 W total input RF power and convective cooling only .

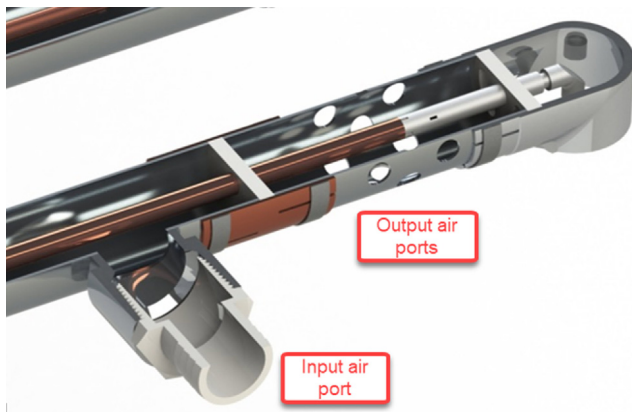


Fig. 19. Cooling input and output ports.

Fine tuning of the resonators is performed through a fine screw adjustment that can be coupled to a servo motor for precision control. This mechanism, however, does not need to be rotationally based, as it is merely to control the depth of the tuner penetration.

The feedthroughs to the beamline chamber consist of two off-the-shelf isolating ceramic feedthroughs welded to a blank CF vacuum flange with 8" outer diameter as shown in Fig. 17. Also welded to this flange are two 304L steel flanged components, machined to receive the EIA 1-5/8" outer conductor. The ceramic feedthroughs have two connectors, manufactured in copper to mimic the standard 7/8" inner conductor connector, brazed to the non-vacuum side of the feedthrough. The vacuum side contains the electrodes brazed to 1/4"

copper rods, accurately positioned with a ceramic spacer and using attachments which provide a small amount of adjustability in the vertical position.

5. Thermal analysis

We performed a thermal analysis of the designed MHB with the input RF power levels provided in Table 3. For simplicity, we did not consider the coaxial resonators bends. As shown in Fig. 18, with a total input RF power of 175 W, when the MHB is cooled only using natural convection, the maximum temperature is 348 °C and the "hot spot" is located on the inner conductor surface of the QWR. The small notches on these plots refer to Teflon supports.

Due to these high temperatures observed in the RF analysis on the inner conductor of the QWR, a cooling system was developed, and the thermal simulation was repeated. It was determined that 20 W/(m² K) of cooling was necessary to keep the inner conductor below 90 °C and maintain the dimensional and frequency stability of the resonator cavities, as discussed in more detail below. The 6 m structure was split into three roughly even legs, each thermally stabilized by forced air convection provided by a commercial blower. The waste air exhausted through ports drilled into the outer conductor that were validated to prevent RF leakage as shown in Fig. 19. Thus, the target peak temperature of 90 °C, a level similar to FRIB MHB [18], was achieved.

The thermal simulations were performed in ANSYS Multiphysics [20]. First, load lines for the input and output were obtained for a single leg of the structure by varying the pressure at the input of the structure. The heat transfer coefficient (h) plotted against flow rate for the convective cooling channel between the conductors was calculated based on the geometry of the structure. Using the calculated load lines and theoretical heat transfer coefficient for the cooling channel, a standard blower was chosen which provides ~45.7 CFM of air flow,

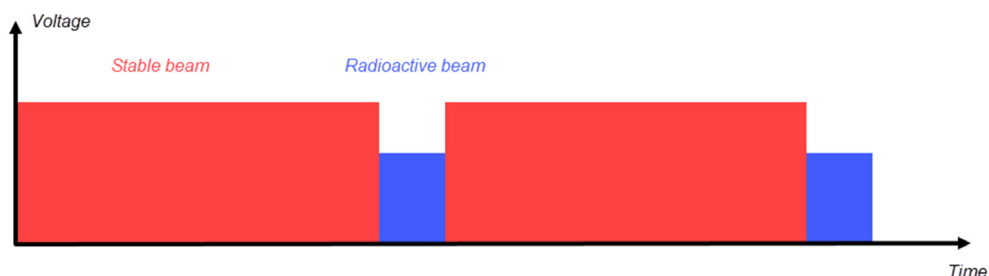


Fig. 20. Time diagram of MHB RF system control voltages.

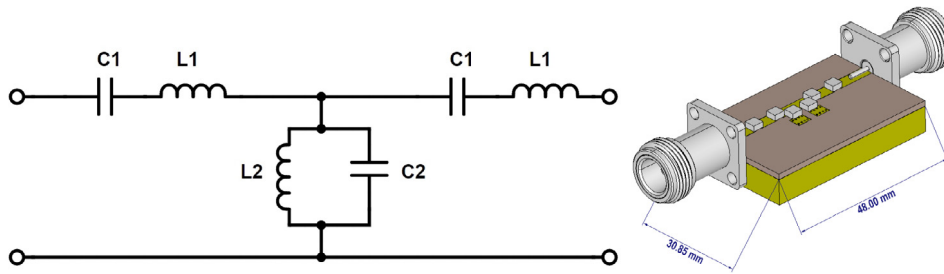


Fig. 23. RF filter scheme (left) and PCB design (right).

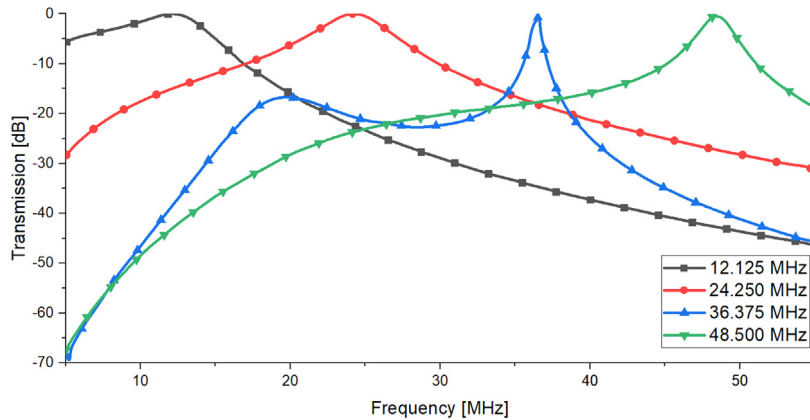


Fig. 24. Filters transmissions as a function of frequency.

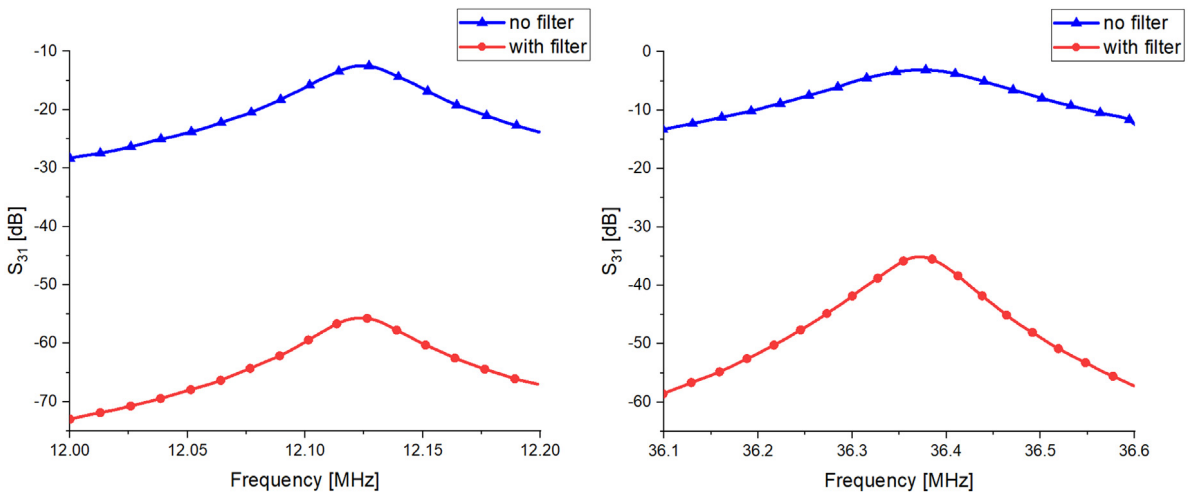


Fig. 25. Cross-talking between 1st and 3rd harmonic ports at 12 MHz (left) and 36 MHz (right) in QWR with and without filters .

board has 4-channel synchronized 500 MS/s digital-to-analog converter output with independent frequency, phase and amplitude control between channels. The benefit of this fully digital system is high stability and better resolution compared to the current analog system used at Argonne, which has 1% amplitude and 1° phase stabilities. DDS features 0.12 Hz frequency resolution, 10-bit output amplitude scaling resolution and 14-bit phase offset resolution, which gives 0.1% amplitude and 0.2° phase stability.

Four solid-state amplifiers driving the MHB (Fig. 22) will be connected downstream to the DDS. The amplitude and phase control of

each amplifier needed for each beam regime will be set through DDS. The feedback signal that measures the electrodes voltage will be used for further stability improvement and monitoring.

Second, to minimize cross-talking and increase isolation between the feeding ports of the MHB, four narrow-band filters (NBF) were designed. Each filter is based on a T-section as shown in Fig. 23. The chosen component values for each frequency are summarized in Table 6.

Fig. 24 shows transmission curves of each filter, demonstrating the good rejection of the undesired harmonics, and Fig. 25 demonstrates the improved isolation between MHB ports when filters are applied. In these

Table 6
Optimal values of the RF filter components as referred in Fig. 23.

| Frequency, MHz | 12.125 | 24.25 | 36.375 | 48.5 |
|----------------|--------|-------|--------|-------|
| L1, nH | 404.3 | 268.6 | 230.2 | 161.1 |
| L2, nH | 22.5 | 7.8 | 4.2 | 3.5 |
| C1, pF | 356.2 | 124.0 | 65.6 | 54.8 |
| C2, nF | 1.59 | 1.06 | 0.91 | 0.64 |

plots, S-parameters are used to describe the input–output relationship between ports. For instance, S_{ab} represents the power transferred from Port b to Port a .

The final modification required for the ANL RF system is the procurement of a fourth power supply for the higher harmonic since Argonne is currently operating with only three power generators.

7. Summary

We have designed a 12 MHz four-harmonic buncher based on coaxial resonators, required to convert ATLAS into a multi-user facility to simultaneously accelerate both stable and radioactive beams. The folded resonator design allows to significantly reduce the dimensions of the system down to ~ 2 m. Fast power switching was implemented to adjust the harmonics voltages required for the simultaneous acceleration of stable and radioactive beams with different intensities.

We optimized the coaxial resonator impedance and the shape of the electrode, so that the cavity has an aperture twice as large as that of the existing cavity. The optimized design and power requirements allow using the existing power system at ATLAS with a minor upgrade. A detailed RF design, including the couplers and tuners, was completed to ensure the cavity operation, stability, and compatibility with the ATLAS power and LLRF systems. We developed the conceptual engineering design and were able to optimize it so that the resonators consist of the maximum number of standard off-the-shelf components, which will reduce the construction cost of the buncher. The conceptual thermal analysis was performed, and the cooling system was developed to ensure the frequency stability of the cavity.

Acknowledgments

This work was supported by the U.S. Department of Energy, Office of Nuclear Physics, under SBIR grant DE-SC0017104.

References

[1] ATLAS website, Available at www.phy.anl.gov/atlas (Accessed on 16 July 2018).

- [2] G. Savard, R. Pardo, Proposal for the 252Cf source upgrade to the ATLAS facility, available at https://www.phy.anl.gov/atlas/caribu/Cf252_upgrade_proposal_final_Rev4.pdf (Accessed on 16 July 2018).
- [3] R.C. Pardo, G. Savard, S. Baker, C. Davids, E. Moore, R. Vondrasek, G. Zinkann, Radioactive beams from ^{252}Cf fission using a gas catcher and an ECR charge breeder at ATLAS, *Nucl. Instrum. Methods Phys. Res.* 261 (2007) 965–968.
- [4] B. Mustapha, J.A. Nolen, G. Savard, P.N. Ostroumov, The ATLAS multi-user upgrade and potential applications, *J. Instrum.* 12 (2017).
- [5] R. Vondrasek, A. Levand, R. Pardo, G. Savard, R. Scott, Charge breeding results and future prospects with electron cyclotron resonance ion source and electron beam ion source, *Rev. Sci. Instrum.* 83 (2) (2012).
- [6] S. Kondrashev, A. Barcikowski, C. Dickerson, R. Fischer, P.N. Ostroumov, R. Vondrasek, A. Pikin, EBIS charge breeder for CARIBU, *Rev. Sci. Instrum.* 85 (2) (2014).
- [7] P.N. Ostroumov, R.V.F. Janssens, M.P. Kelly, S.A. Kondrashev, B. Mustapha, R.C. Pardo, G. Savard, Efficiency and intensity upgrade of the ATLAS facility, in: *Proc. Linear Accelerator Conference LINAC2010*, Tsukuba, Japan, MOP045.
- [8] S. Sharamentov, P. Ostroumov, private communications.
- [9] L.M. Bollinger, R.C. Pardo, K.W. Shepard, P.J. Billquist, J.M. Bogaty, B.E. Clift, R. Harkewicz, F.H. Munson, J.A. Nolen, G.P. Zinkann, The positive-ion injector of ATLAS: design and operating experience, *Nucl. Instrum. Methods Phys. Res. B* 79 (1–4) (1993) 753–757.
- [10] P.N. Ostroumov, Z. Conway, C. Dickerson, S. Gerbick, M. Kedzie, M. Kelly, S.H. Kim, Y. Luo, S. MacDonald, R. Murphy, B. Mustapha, R. Pardo, T. Reid, S. Sharamentov, K. Shepard, J. Specht, G. Zinkann, A. Perry, Completion of efficiency and intensity upgrade of the ATLAS Facility, in: *Proc. of Linear Accelerator Conference LINAC2014*, Geneva, Switzerland, TUPP005.
- [11] F.J. Lynch, R.N. Lewis, L.M. Bollinger, W. Henning, O.D. Despe, Beam buncher for heavy ions, *Nucl. Instrum. Methods* 159 (23) (1979) 245–263.
- [12] S. Sharamentov, J. Bogaty, B.E. Clift, R. Pardo, Upgrade of the ATLAS positive ion injector bunching system, in: *Proc. of the Particle Accelerator Conference PAC05*, Knoxville, TN, May 16–20, 2005, pp. 2161–2163.
- [13] P.N. Ostroumov, V.N. Aseev, A. Barcikowski, B. Clift, R. Pardo, S.I. Sharamentov, M. Sengupta, Beam test of a grid-less multi-harmonic buncher, in: *Proc. of Particle Accelerator Conference PAC07*, Albuquerque, New Mexico, USA, 2017, WEPMN091.
- [14] J. Holzbauer, W. Hartung, F. Marti, E. Pozdeyev, Q. Zhao, Electromagnetic design of a multi-harmonic buncher for the FRIB driver linac, in: *Proceedings of Particle Accelerator Conference PAC11*, New York, NY, USA, TUP091.
- [15] Electronic Components Industry Association website, available at <http://www.ecianow.org> (Accessed on 16 July 2018).
- [16] Computer Simulation Technology website, available at <https://www.cst.com> (Accessed on 16 July 2018).
- [17] V.N. Aseev, P.N. Ostroumov, E.S. Lessner, B. Mustapha, TRACK: The new beam dynamics code, in: *Proc. of the Particle Accelerator Conference PAC05*, Knoxville, TN, May 16–20, 2005, p. 2053.
- [18] E. Pozdeyev, J. Brandon, N. Bultman, X. Rao, R. York, Q. Zhao, Report on design, development, and characterization of a coaxial resonator based single-gap gridless multiharmonic buncher, available at <https://www.osti.gov/servlets/purl/1073065> (Accessed 16 July 2018).
- [19] S. Lal, K.K. Pant, Study of the effect of loop inductance on the RF transmission line to cavity coupling coefficient, *Rev. Sci. Instrum.* 87 (2016) 083308.
- [20] ANSYS website, available at <https://www.ansys.com> (Accessed on 16 July 2018).